Radar interferometric phase errors induced by Faraday rotation

Simon Zwieback, Franz J. Meyer, *Senior Member, IEEE*

***Abstract*—Ionospheric Faraday rotation distorts satellite radar observations of the Earth's surface. While its impact on radiometric observables is well understood, the errors in repeat-pass InSAR observations and hence in deformation analysis are largely unknown. Because Faraday rotation cannot rigorously be compensated for in non-quad-pol systems, it is imperative to determine the magnitude and nature of the deformation errors. Focusing on distributed targets at L-band, we assess the errors for a range of land covers using airborne observations with simulated Faraday rotation.**

We find that the deformation error may reach 2 mm in the co-pol channels over a solar cycle. It can exceed 5 mm for intense solar maxima. The cross-pol channel is more susceptible to severe errors. We identify the leakage of polarimetric phase contributions into the interferometric phase as a dominant error source. The polarimetric scattering characteristics induce a systematic dependence of the Faraday-induced deformation errors on land cover and topography. Also their temporal characteristics, with pronounced seasonal and quasi-decadal variability, predispose these systematic errors to be misinterpreted as deformation. While the relatively small magnitude of 1–2 mm is of limited concern in many applications, the persistence on semi- to multi-annual time scales compels attention when long-term deformation is to be estimated with millimetric accuracy. Phase errors induced by uncompensated Faraday rotation constitute a non-negligible source of bias in interferometric deformation measurements.

I. Introduction

Microwaves propagating through the ionosphere are subject to Faraday rotation, which manifests as a rotation of the polarization plane of linearly polarized waves [1], [2]. Equivalently, the Earth's magnetic field turns the ionospheric plasma into a circularly birefringent medium [3], [4]. Left- and right-circularly-polarized waves propagate at slightly different phase velocities. The Faraday effect's magnitude increases with the total electron content (TEC) in the ionosphere [3], [5]. It also depends on the frequency. Spaceborne observations at frequencies below $\sim$3 GHz are affected most significantly, with one-way Faraday angles χ of up to 30° at L-band [6].

There is insufficient information in single- or dual-pol data to rigorously correct for Faraday rotation. This is in contrast to quad-pol observations, for which numerous physically based correction approaches have been devised [1], [2]. In analyses dealing with single- or dual-pol observations, usually no attempt is made to correct for Faraday rotation.

Uncompensated Faraday rotation distorts interferometric observations, as well as those of backscatter magnitudes and polarimetric parameters [6], [7]. While these latter have been studied in detail, the Faraday-induced errors in interferometric analyses of distributed targets have received scant scrutiny [8], [6]. Reductions in the interferometric coherence due to Faraday rotation have been reported, their magnitudes varying with the target scattering characteristics [6]. Conversely, we lack a clear picture of the controls and magnitude of the Faraday-induced errors in the interferometric phase. There is a need to quantify how the Faraday-induced phase errors distort deformation estimated using InSAR (interferometric synthetic aperture radar). The upcoming L-band InSAR satellite mission NISAR [9] aims to estimate secular deformation with a high accuracy of better than 2 mm per year, which necessitates a sound understanding of even minor error terms such as Faraday rotation.

Our objectives are to

- identify the magnitude and nature of the Faraday-induced phase errors
- assess their relevance for InSAR deformation measurements

To identify their magnitude, we evaluate the errors for a range of land covers using airborne L-band observations with simulated Faraday rotation. Adding simulated Faraday rotation to observations undistorted by ionospheric errors is a compelling approach for quantifying errors because we have a sound mechanistic understanding of Faraday rotation [10], [1], [6]. We quantify the co-pol and cross-pol errors in the observed interferometric phase ϕ and in the split-spectrum ionospherically corrected phase ϕ^c. Both are relevant to deformation analyses [11], as the Faraday-induced errors in the displacement estimates will closely follow those in ϕ and ϕ^c on small and large spatial scales, respectively. To characterize the nature of the errors, we theoretically analyze the errors as a function of the target scattering characteristics. We identify two contributions: the leakage of polarimetric phases into the interferometric phase; and the polarimetric diversity of the interferometric phase [12].

To assess the relevance for InSAR deformation measurements, we characterize the temporal and spatial properties of the errors. We find that the temporal characteristics, inferred from a multi-annual time series, mimic those of real deformation processes, with systematic variations on seasonal to multi-annual time scales. Spatially, the errors vary systematically with land cover and topography, a pattern that can largely be explained by polarimetric leakage. The systematic nature of the Faraday-induced errors implies that they cannot be mitigated by simple filtering. We conclude that the magnitude of

Both authors are with the Geophysical Institute, University of Alaska Fairbanks. This work was supported by the National Aeronautics and Space Administration (NASA) under Grants 80NSSC19K1494 and NNH18ZDA001N-RST.

up to 2 mm and the pernicious spatiotemporal characteristics of these errors necessitate their inclusion in error budgets. We thus outline a way forward on how to mitigate their influence in geodetic deformation analyses.

II. Theoretical considerations

A. Faraday rotation

The magnitude of the ionospheric Faraday rotation angle χ is inversely proportional to the square of the signal frequency f. L-band observations are subject to Faraday effects that are approximately 20 times larger than at C-band. The magnitude further depends on the observation geometry and the magnetic field. [1] derived the following approximate relation

$$\chi = \frac{K}{f^2} B \frac{\cos(\psi)}{\cos(\theta)} \mathrm{TEC} \tag{1}$$

where K is a constant and B is the scalar magnetic flux density in the ionosphere. ψ the angle between the wave vector and the Earth's magnetic field, θ the incidence angle, and TEC the total electron content in the ionosphere.

Ionospheric Faraday rotation is subject to pronounced spatial and temporal variability. Faraday rotation is minimal near the geomagnetic equator because of the $\cos(\psi)$ factor. In mid- and high-latitude regions, Faraday rotation angles can exceed 10° at L-band for spaceborne observation geometries. TEC fluctuations cause the Faraday rotation angles to vary diurnally, seasonally, and with solar activity. The largest values of approximately 30° are expected to preferentially occur in mid-latitudes during solar maxima [1]. While such extreme values are rare, [1] estimate Faraday rotation to exceed 10° more than half the time along an orbit. Weak solar maxima such as the 2013 maximum are associated with χ approximately half as large. During solar minima, χ rarely exceeds 5° [1].

B. Interferometric covariance matrix

The ionospheric Faraday effect alters the microwave signals a radar satellite receives and hence the apparent scattering properties of the Earth's surface.

Its impact on the interferometric covariance matrix $\mathbf{C}$ [13] is described by

$$\begin{aligned} &{}_F\mathbf{C}(\chi_1,\chi_2) = \\ &\begin{bmatrix} \mathbf{R}_F(\chi_1) & \\ & \mathbf{R}_F(\chi_2) \end{bmatrix} \begin{bmatrix} \mathbf{\Sigma}_1 & \mathbf{\Omega} \\ \mathbf{\Omega}^\dagger & \mathbf{\Sigma}_2 \end{bmatrix} \begin{bmatrix} \mathbf{R}_F(\chi_1) & \\ & \mathbf{R}_F(\chi_2) \end{bmatrix}^T \end{aligned} \tag{2}$$

where

$$\mathbf{R}_F(\chi) = \begin{bmatrix} \cos(2\chi) & 0 & 0 & -\sin(2\chi) \\ 0 & 1 & 0 & 0 \\ 0 & 0 & 1 & 0 \\ \sin(2\chi) & 0 & 0 & \cos(2\chi) \end{bmatrix}$$

is a unitary matrix [1], [6]. $\mathbf{\Sigma}_1$ and $\mathbf{\Sigma}_2$ are the polarimetric covariance matrices of acquisitions 1 and 2, respectively, whereas the off-diagonal block $\mathbf{\Omega}$ contains the interferometric information. Equation (2) is given in the Pauli basis of the quad-pol scattering vector [13] in the backscattering alignment convention, i.e. $\mathbf{k} = \frac{1}{\sqrt{2}}\left[S_{\mathrm{HH}} + S_{\mathrm{VV}} \quad S_{\mathrm{HH}} - S_{\mathrm{VV}} \quad S_{\mathrm{HV}} + S_{\mathrm{VH}} \quad \mathrm{i}\,(S_{\mathrm{HV}} - S_{\mathrm{VH}})\right]^T$. We will use the Pauli basis for our theoretical analyses because the simple form of $\mathbf{R}_F(\chi)$ streamlines the expressions.

The Faraday-affected interferometric phase ${}_F\phi$ for polarimetric measurement functionals $\mathbf{w}_1^\dagger$ and $\mathbf{w}_2^\dagger$ – linear functionals are denoted by row vectors that act through the standard inner product – is then given by

$${}_F\phi = \arg\left(\mathbf{w}_1^\dagger \mathbf{R}_F(\chi_1) \mathbf{\Omega} \mathbf{R}_F^T(\chi_2) \mathbf{w}_2\right). \tag{3}$$

To isolate purely interferometric signals from what are essentially polarimetric phase contributions [14], one generally chooses $\mathbf{w}_1^\dagger = \mathbf{w}_2^\dagger \equiv \mathbf{w}^\dagger$ to obtain a phase $\phi_{\mathbf{w}^\dagger}$. In presence of unequal uncompensated Faraday rotation however, the interferogram is then effectively formed from two different channels. It can be thought of as the result of a Faraday-free covariance matrix $\mathbf{C}$ observed with two distinct functionals $\mathbf{w}^\dagger \mathbf{R}_F(\chi_1) \neq \mathbf{w}^\dagger \mathbf{R}_F(\chi_2)$. .

C. Phase errors

The Faraday-induced interferometric phase error is defined to be the difference between the Faraday-affected phase ${}_F\phi_{\mathbf{w}^\dagger}$ and the Faraday-free phase $\phi_{\mathbf{w}^\dagger}$.

$${}_F\delta\phi_{\mathbf{w}^\dagger} \equiv {}_F\phi_{\mathbf{w}^\dagger} - \phi_{\mathbf{w}^\dagger}. \tag{4}$$

We identify two contributions to the phase error ${}_F\phi_{\mathbf{w}^\dagger}$. The first one is the polarimetric leakage that arises from forming an interferogram from two distinct channels whenever $\chi_1 \neq \chi_2$. It is the only contribution and thus identical to the overall error ${}_F\phi_{\mathbf{w}^\dagger}$ when the Faraday-unaffected $\mathbf{\Omega}$ is phase invariant, i.e. when the interferometric phase does not depend on $\mathbf{w}^\dagger$ (see Sec. VII). The second contribution arises from the phase diversity of $\mathbf{\Omega}$, i.e. when $\mathbf{\Omega}$ is not phase invariant. It induces errors even when $\chi_1 = \chi_2 \neq 0$.

The total phase error cannot be neatly decomposed into the two contributions whenever $\mathbf{\Omega}$ is not phase invariant and $\chi_1 \neq \chi_2$. They are both present at the same time and interact nonlinearly on ${}_F\delta\phi_{\mathbf{w}^\dagger}$. It is mathematically expedient to focus on polarimetric leakage errors (for phase-invariant $\mathbf{\Omega}$, i.e. no phase diversity) and the overall error (for general $\mathbf{\Omega}$). We have summarized the key theoretical properties of the error types in Tab. I.

1) Polarimetric leakage: Polarimetric leakage for phase-invariant $\mathbf{\Omega}$ is a confounding of the interferometric phase signal with polarimetric phase contributions. It arises when $\chi_1 \neq \chi_2$, as one then forms an interferogram from two distinct channels. We define it as the Faraday-induced phase error for a phase-invariant $\mathbf{\Omega} = \mathrm{e}^{\mathrm{i}\tilde{\phi}}\tilde{\mathbf{\Omega}}$ from Sec. VII:

$${}_F\delta\phi^{\mathrm{pol}}_{\mathbf{w}^\dagger} \equiv \arg\left(\mathbf{w}^\dagger \mathbf{R}_F(\chi_1) \tilde{\mathbf{\Omega}} \mathbf{R}_F^T(\chi_2) \mathbf{w}\right). \tag{5}$$

It only depends on the Hermitian matrix $\mathbf{\Omega}$, which only contains polarimetric phases. For equal Faraday rotation, $\chi_1 = \chi_2$, this error vanishes because $\mathbf{\Omega}$ is positive (semi-)definite. When $\chi_1 \neq \chi_2$, polarimetric phases from the off-diagonal elements $\tilde{\mathbf{\Omega}}$ leak into the interferometric phase.

The polarimetric leakage errors tend to accumulate along interferogram chains. Even if the difference in χ is small for

TABLE I
SUMMARY OF THEORETICAL RESULTS. THE POLARIMETRIC LEAKAGE ERROR ${}_F\delta\phi^{\mathrm{pol}}$ IS EQUAL TO THE PHASE ERROR ${}_F\delta\phi_{\mathbf{w}^\dagger}$ WHEN $\mathbf{\Omega}$ IS PHASE INVARIANT. IF $\mathbf{\Omega}$ IS NOT PHASE INVARIANT, CONTRIBUTIONS FROM POLARIMETRIC LEAKAGE AND PHASE DIVERSITY INTERACT NONLINEARLY. THE SPLIT-SPECTRUM ERROR EQ. 15 IS THE TOTAL ERROR OF THE IONOSPHERICALLY CORRECTED PHASE ϕ^c.

Error type	Property of Faraday-induced error
Polarimetric leakage ${}_F\delta\phi^{\mathrm{pol}}$	defined for phase-invariant $\mathbf{\Omega}$ vanishes for $\chi_1 = \chi_2$ leading order of χ dependence: 2 (co-pol) and 1 (cross-pol) cross-pol: vanishes for reflection symmetry across $\mathcal{P}_V$ accumulates along interferogram chains
Phase error ${}_F\delta\phi$	nonlinear combination of phase diversity and polarimetric leakage does not vanish when $\chi_1 = \chi_2$ leading order of χ dependence: 2 (co-pol) and 1 (cross-pol)
Split-spectrum errors ${}_F\delta\phi^c$	same order of magnitude as ${}_F\delta\phi$ for $\Delta f' \ll 1$

individual short-term interferograms, the errors add up over time, as demonstrated in Sec. VIII.

To understand the polarimetric leakage error in general $\mathbf{\Omega}$, we introduce a phase-invariant approximation $\mathbf{\Omega}'$. It is useful for constraining the nature of the errors, but it does not amount to a decomposition of the phase errors because the two components interact nonlinearly. To obtain $\mathbf{\Omega}'$, we first remove an average interferometric phase $\phi' = \arg(\mathrm{tr}\mathbf{\Omega})$ and extract the Hermitian component:

$$\mathbf{\Omega}'_{\mathrm{H}} = \frac{1}{2}\left(\mathrm{e}^{-\mathrm{i}\phi'}\mathbf{\Omega} + \mathrm{e}^{\mathrm{i}\phi'}\mathbf{\Omega}^\dagger\right), \tag{6}$$

which would be positive (semi-)definite if $\mathbf{\Omega}$ were phase invariant to begin with. We enforce positive-(semi-)definiteness using the PSD operator that sets any negative eigenvalues to zero, and then reapply ϕ':

$$\mathbf{\Omega}' = \mathrm{e}^{\mathrm{i}\phi'}\,\mathrm{PSD}\,(\mathbf{\Omega}'_{\mathrm{H}}) \tag{7}$$

2) Total errors: When $\mathbf{\Omega}$ is not phase invariant, the phase diversity will also contribute to the total error. It interacts nonlinearly with polarimetric leakage when $\chi_1 \neq \chi_2$ because of the nonlinear argument operation in (3). Mathematically, it is natural to focus on the complex scalar $\mathbf{w}^\dagger\mathbf{R}_F(\chi_1)\mathbf{\Omega}\mathbf{R}_F^T(\chi_2)\mathbf{w}$. By decomposing $\mathbf{\Omega}$ into $\mathbf{\Omega}'$ (polarimetric leakage) and a remainder (phase diversity), we obtain a linear superposition. But in practice we are interested in the phase, so we restrict our attention to the combined impact of the two error contributions.

The physical significance of the phase-diversity error can be seen most clearly when $\chi_1 = \chi_2$. Provided both scenes are affected by non-zero Faraday rotation, one forms an interferogram in the wrong channel. Its phase will then generally differ from that of the Faraday-free scenario because of the phase diversity of $\mathbf{\Omega}$.

3) Co-pol phase errors: We now derive explicit expressions and approximations for the co-pol phase error. Expressing $\mathbf{\Omega}$ in the Pauli basis and assuming reciprocity in the absence of Faraday rotation [13], one obtains from (4)

$${}_F\phi_{\mathrm{HH/VV}} = \arg\Big[\Omega_{22} + \Omega_{11}\cos(2\chi_1)\cos(2\chi_2) \pm \Omega_{12}\cos(2\chi_1) \pm \Omega_{21}\cos(2\chi_2)\Big]. \tag{8}$$

The plus and minus of the $\pm$ sign refer to HH and VV, respectively.

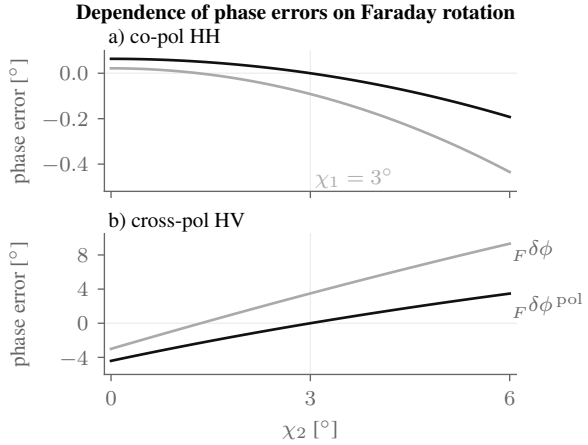

Fig. 1. Faraday-induced phase errors ${}_F\delta\phi$ for general $\mathbf{\Omega}$ and the polarimetric leakage errors ${}_F\delta\phi^{\mathrm{pol}}$ for phase-invariant $\mathbf{\Omega}$ are shown for an agricultural field in a) HH and b) HV polarization. χ_1 was set to 3°. The $\mathbf{\Omega}$ observation was taken from stack `31606` (Tab. II); the phase-invariant component was computed from the Hermitian/skew-Hermitian decomposition (Sec. III-C)

The error with respect to the Faraday-free phase, $\phi_{\mathrm{HH/VV}}$, is of second order in the Faraday rotation angles

$$\begin{aligned}{}_F\delta\phi_{\mathrm{HH/VV}} &= {}_F\phi_{\mathrm{HH/VV}} - \phi_{\mathrm{HH/VV}} \\ &= \mp 2\frac{\mathrm{Im}\,(t_c\Omega_{12})\,\chi_1^2 + \mathrm{Im}\,(t_c\Omega_{21})\,\chi_2^2}{\mathrm{Re}\,(t_c\,(\Omega_{11}+\Omega_{22}\pm\Omega_{12}\pm\Omega_{21}))} + o\left(\chi^3\right),\end{aligned} \tag{9}$$

using $t_c = \mathrm{e}^{-\mathrm{i}\phi_{\mathrm{HV/VV}}}$ and assuming phase wrapping is not an issue.

The second-order χ dependence of the co-pol phase error is illustrated in Fig. 1a for an agricultural field. It does not vanish when $\chi_1 = \chi_2$ because it contains phase diversity and polarimetric leakage components.

For a phase-invariant $\tilde{\mathbf{\Omega}}$, the error is entirely due to polarimetric leakage and is given by

$${}_F\delta\phi^{\mathrm{pol}}_{\mathrm{HH/VV}} = \mp 2\frac{\mathrm{Im}\left(\tilde{\Omega}_{12}\right)\left(\chi_1^2 - \chi_2^2\right)}{\tilde{\Omega}_{11} + \tilde{\Omega}_{22} \pm 2\mathrm{Re}\left(\tilde{\Omega}_{12}\right)} + o\left(\chi^3\right). \tag{10}$$

The leading-order term $\chi_1^2 - \chi_2^2$ induces asymmetry in the Faraday-induced error (Fig. 1a). For fixed $\chi_1 > 0$, ${}_F\delta\phi^{\mathrm{pol}}_{\mathrm{HH/VV}}$ increases more rapidly in magnitude for $\chi_2 > \chi_1$ than it does for $\chi_2 < \chi_1$. The error vanishes when $\chi_1 = \chi_2$.

The polarimetric origin of this error is most evident when $\tilde{\mathbf{\Omega}} = \mathbf{\Sigma}_1 = \mathbf{\Sigma}_2 \equiv \mathbf{\Sigma}$, i.e. in absence of any interferometric changes between acquisitions one and two (other than Faraday rotation). The error is controlled by $\mathrm{Im}\,(\Sigma_{12})$. This term, along with the associated phase $\arg(\Sigma_{12})$, is known to be difficult to predict when both surface and volume scattering are appreciable [15]. Simple models, such as the small-perturbation model for surface scattering and volume models with azimuthal symmetry [13], predict a small (compared to Σ_{11}) or even vanishing magnitude, and are thus prone to underestimating its size. Azimuth slopes θ reduce the $\mathrm{Im}\,(\Sigma_{12})$ term by $\cos 2\theta$ for an otherwise reflection-symmetric target [16], so that flat terrain is expected to have comparatively large co-pol polarimetric leakage errors.

4) Cross-pol phase errors: For a reciprocal target, the cross-pol phase error from Eq. 4 can be expressed as

$$ {}_F\phi_{\mathrm{HV/VH}} = \arg\Big[\Omega_{33} + \Omega_{11}\sin(2\chi_1)\sin(2\chi_2) \mp \Omega_{13}\sin(2\chi_1) \mp \Omega_{31}\sin(2\chi_2)\Big]. \quad (11)$$

Faraday rotation thus induces first-order errors with respect to $\phi_{\mathrm{HV}} = \phi_{\mathrm{VH}}$, viz.

$$ {}_F\delta\phi_{\mathrm{HV/VH}} = \mp 2\frac{\mathrm{Im}\,(t_x\Omega_{13})\,\chi_1 + \mathrm{Im}\,(t_x\Omega_{31})\,\chi_2}{\mathrm{Re}\,(t_x\,(\Omega_{33}))} + o\,(\chi)\ , \quad (12)$$

using $t_x = \mathrm{e}^{-\mathrm{i}\phi_{\mathrm{HV}}}$. For fixed χ_1, the error can be approximated by a linear function in χ_2 near χ_1 (Fig. 1b).

The cross-pol errors are expected to be small for flat terrain, or more precisely for targets with reflection symmetry across the plane $\mathcal{P}_V$ formed by the line of sight and the vertical polarization direction [16]. This is because i) polarimetric leakage is zero due to $\Omega_{13} = \Omega_{31} = 0$ [13], and ii) the phase-diversity error arising from $\arg(\Omega_{33}) \neq \arg(\Omega_{11})$ is only of second order in χ.

Conversely, the errors can be substantial when the terrain is tilted in azimuth. We consider a target that is reflection symmetric across $\mathcal{P}_V$ with phase-invariant $\tilde{\mathbf{\Omega}}^r$. If the target is tilted by θ in azimuth, the Faraday-induced phase error increases with θ as

$$ {}_F\delta\phi^{\mathrm{pol}}_{\mathrm{HV/VH}} = \pm 2\frac{\sin(2\theta)\mathrm{Im}\left(\tilde{\Omega}^r_{12}\right)}{\tilde{\Omega}^r_{22}\sin(2\theta)^2 + \tilde{\Omega}^r_{33}\cos(2\theta)^2}\,(\chi_1 - \chi_2) + o(\chi). \quad (13)$$

The rate at which this polarimetric leakage error increases with θ is determined by the ratio of the imaginary part of $\tilde{\Omega}^r_{12}$ and the cross-pol magnitude $\tilde{\Omega}^r_{33}$. For sparsely vegetated areas, the low magnitude and coherence of the cross-pol return will tend to increase this ratio and accentuate phase errors in rolling terrain.

D. Split-spectrum errors

1) Split-spectrum correction: Split-spectrum analyses serve to estimate and remove the ionospheric phase screen [17], [11]. Their rationale is to exploit the dispersive nature of the ionospheric phase screen by quantifying interferometric phase differences across spectral sub-bands [3].

Faraday rotation may bias split-spectrum analyses when the Faraday-induced ${}_F\delta\phi$ in the sub-bands propagate to the ionospherically corrected phase. The bias in turn depends on how ${}_F\delta\phi$ changes with frequency. Frequency-dependent ${}_F\delta\phi$ arises because i) Faraday rotation angles and ii) the $\mathbf{\Omega}$ matrix (other than multiplication by a scalar) vary with frequency.

A potential additional source of frequency-dependent errors are iii) sub-band differences in polarization. In the quasi-quadpol mode under consideration for NISAR, the main band with HH and HV polarizations would be complemented by a sideband with VV and VH polarizations [9]. Then, differences in polarization that arise directly from phase diversity (e.g. an HH–VV phase difference associated with birefringence in agricultural canopies [12], [18]) or from the polarization-dependent impact of Faraday rotation (HV vs. VH) could distort the ionospheric correction.

Our theoretical analyses focus on the errors in the ionosphere-corrected phase ϕ^c at frequency $f = f_0$ obtained by split-spectrum analysis [11]. The spectrum is split into a lower band with $f = f'_- f^0$ and an upper band with $f = f'^+ f_0 \equiv (f'^- + \Delta f')f^0$, whose interferometric phase observations are denoted as ϕ^- and ϕ^+, respectively. The corrected phase ϕ^c is given by [17]

$$ \phi^c = \frac{\phi^+ f'^+ - \phi^- f'^-}{\Delta f'\ (f'^+ + f'^-)}\,. \quad (14)$$

There is a definitional ambiguity in the corrected phase ϕ^c and in ionospheric corrections more generally. For non-zero Faraday rotation, the ionospheric phase depends on the target and the polarimetric functional. To estimate and interpolate the ionospheric phase, one needs to resort to convention. We adopt the standard convention that defines the ionospheric phase to be removed as that of the co-polar circular channels LL and RR [19]. This is also the delay for a pure idealized dihedral (Pauli 2) or a pure cross-pol (Pauli 3) signal when measured with the associated polarimetric functional [13]. As a metric of the ambiguity, we define $\Gamma = 2|\chi_2 - \chi_1|$, the magnitude of the deviation in the ionospheric phase delay between a pure Left-Right (LR) or an RL scatterer, neither of which is reciprocal.

The corrected phase ϕ^c is more of theoretical than of practical value. In practice, it can only be estimated at the reduced resolution of ϕ^- and ϕ^-. To retain the full resolution, actual implementations instead subtract a smoothed split-spectrum ionospheric estimate from the full-resolution phase. The two corrections are equivalent when the scattering characteristics are uniform across the ionospheric smoothing filter. With our focus on ϕ^c, we thus implicitly concentrate on homogeneous environments. Conversely, at length scales smaller than size of the smoothing filter, the Faraday-induced error will be dominated by that of the raw phase, ${}_F\delta\phi$.

2) Error analysis: The split-spectrum ionospheric corrected phase is impacted by frequency-varying and frequency-invariant phase errors to a different extent [11]. Phase errors in the upper and lower band propagate into the split-spectrum corrected phase from 14 as

$$ \delta\phi^c = \frac{(\delta\phi^+ - \delta\phi^-)\,f'^- + \delta\phi^+\Delta f'}{\Delta f'\,(2f'^- + \Delta f')}\,. \quad (15)$$

Roughly speaking, frequency-invariant errors are halved, whereas differences between the bands $\Delta\delta = \delta\phi^{+} - \delta\phi^{-}$ get amplified substantially, by a factor of $\approx (2\Delta f')^{-1}$.

The contributions from frequency-varying and frequency-invariant Faraday errors to $\delta\phi^{c}$ are of the same order of magnitude. This is because the $\Delta\delta$ term that gets amplified is small, as it generally scales as $\Delta f'$. We consider identical sub-band polarizations and assume that i) the frequency-dependence of Faraday errors is the only cause for diverging Faraday-induced errors in the sub-bands. As $\chi \sim f'^{-2}$ (1), $\Delta\delta \sim 2\Delta f'$ in the cross-pol channel (first-order scaling of the Faraday errors), while it is proportional to $4\Delta f'$ for the co-pol channel (second-order errors).

The Faraday error in the corrected phase ϕ^{c} and the raw phase ϕ are of the same order of magnitude, provided that the same polarization is used for both subbands. This is because the frequency-varying and frequency-invariant contributions are of the same order of magnitude, the latter corresponding to the error of the raw phase. If the two contributions are of opposite sign, partial cancellation can occur.

A radically different picture emerges for quasi-quadpol systems. The inter-band error $\Delta\delta$ is then also due to iii) polarization differences, and its potentially large magnitude gets further amplified by a large factor of approximately $(2\Delta f')^{-1}$.

III. Observational analyses

A. Faraday-free radar observations

We studied five fully polarimetric SLC stacks, summarized in Tab. II, acquired by NASA's L-band UAVSAR system [20]. These airborne data are not affected by ionospheric distortions.

We estimated the interferometric covariance matrix by boxcar multilooking with $L = 100$ looks, obtaining a resolution of $\sim$10 m. To ensure the polarimetric fidelity of the observations, we zeroed the Pauli 4 return for each SLC pixel. This enforces scattering reciprocity, as assumed throughout Sec. II.

The polarimetric calibration of the UAVSAR data is reliable and stable [20]. Among the five calibration parameters, the copol channel imbalance and phase offset are critical because they impact the Ω_{12} term in 10. While we could not assess them independently in absence of calibration targets, we could investigate forests. The Faraday-induced phase errors in (10) vanish to leading order for azimuthally symmetric targets such as dense forests. If, conversely, polarimetric calibration error dominated the results obtained using (10), the error estimates over forests would cease to be small compared to those over other land covers. The data do not point to dominant polarimetric calibration errors over forests.

B. Quantifying phase errors by adding Faraday rotation

To estimate the Faraday-induced co-pol and cross-pol phase errors ${}_{F}\delta\phi$, we simulated Faraday-affected interferometric pairs with a temporal baseline of 1–3 weeks using (2). The phase errors ${}_{F}\delta\phi$ were estimated by subtracting the Faraday-unaffected from the Faraday-affected phase.

The Faraday rotation angles χ_1 and χ_2 were chosen to cover the range of potential values at L-band [6]. For most analyses, we focused on four values, namely 0° (none), 3° (weak), 10° (strong), and 30° (maximum). An interferogram formed from scenes with 0° and 30°, corresponding to a strong solar maximum, is intended to bound the maximum errors that may reasonably be expected in the mid-latitudes [1], [6]. Weak and strong Faraday rotation represent seasonally and diurnally averaged conditions over the course of a solar cycle, during the solar minimum and maximum, respectively [1].

C. Magnitude and nature of Faraday-induced phase errors

To assess how the Faraday-induced errors vary with land cover, we summarized the mean ${}_{F}\delta\phi$ values for each interferogram across multiple regions of interest for three land cover classes (Tab. II): agricultural, sparsely vegetated (scrub, wetlands, clearcuts), and forest.

To quantify the ${}_{F}\delta\phi$ contribution from polarimetric leakage relative to that induced by phase diversity, we estimated ${}_{F}\delta\phi^{\mathrm{pol}}$ for the phase-invariant approximation $\mathbf{\Omega}'$ of (6).

We assessed the association of the cross-pol errors with deviations from reflection symmetry. We estimated the orientation angle θ for tilted reflection-symmetric targets [16] and the Pauli 1–Pauli 3 polarimetric coherence $\rho_{13} = |\Sigma_{13}|\,(\Sigma_{11}\Sigma_{33})^{-\frac{1}{2}}$, which is zero for reflection symmetry across $\mathcal{P}_V$.

D. Simulated temporal evolution of Faraday-induced errors

The temporal evolution of the Faraday-induced phase error was simulated using Faraday rotation angles χ derived from the International GNSS Service (IGS) TEC products. We extracted the final combined IGS TEC [21] estimate evaluated at the site of the Californian UAVSAR stack at 5 pm local time every 11 days, roughly corresponding to the late afternoon acquisitions of a sun-synchronous satellite. From these TEC estimates, we computed χ using the expression by [1] for a polar L-band satellite with an incidence angle of 30°.

We estimated the Faraday-induced errors with respect to the first acquisition due to polarimetric leakage alone, ${}_{F}\delta\phi^{\mathrm{pol}}$, using a fixed phase-invariant $\mathbf{\Omega}$ derived from the UAVSAR observations. We focused on the polarimetric leakage error because it is often the dominant contribution, and because we lack long-term observations to characterize the phase diversity adequately. Furthermore, by using a single phase-invariant covariance matrix, the impact of the arbitrary choice of adding up 11-day interferograms to obtain a long time series is minimized for dominant surface scattering. This is because polarimetric leakage does not induce closure errors [22] for rank-one $\mathbf{\Omega}$ (see Sec. VIII).

E. Split-spectrum errors

We estimated the impact of Faraday rotation on the split-spectrum ionospheric correction for an L-band system such as NISAR [9]. The system parameters were given by $f^0 = 1.243$ GHz, $f'^{-} = 1.0$, $f'^{+} = 1.02$. We assumed that $\mathbf{\Omega}(f') = \exp \mathrm{i}\phi(f'))\mathbf{\Omega}(f^0)$, thus neglecting changes in intensity, polarimetric phases, and coherence magnitudes as well as in polarimetric interferometric phase differences with frequency.

TABLE II
THE LOCATION, DOMINANT LAND COVER, UAVSAR STACK NUMBER, AND THE NUMBER $N.$ OF STUDIED REGIONS OF INTEREST WITH CROPS (N_c), SPARSE VEGETATION (N_s) OR FOREST COVER (N_f).

Location			Stack	Land cover	N_c	N_s	N_f
California, USA	31.1N	122.2W	05508	semiarid scrub, wetland	0	3	0
Manitoba, Canada	49.6N	98.0W	31606	fields: cereals, oilseeds	5	0	1
Quebec, Canada	46.8N	71.1W	18801	forest, clearcuts, fields	1	2	2
Maine, USA	45.1N	68.6W	16701	mixed forest	0	0	4
Estuaire, Gabon	0.5N	9.5E	27080	tropical rain forest	0	0	1

We further assumed the interferometric phase differences between any two $\mathbf{w}^\dagger$ were less than 2π in magnitude. Under these assumptions, we assessed the split-spectrum phase errors for same-polarization split-spectrum analyses (HH, HV) but also for the quasi-quadpol mode combinations proposed for NISAR (HH-VV, HV-VH).

The error due to Faraday rotation, ${}_F\delta\phi^c$, was computed using (15) from the ${}_F\delta\phi$ phase errors in the two bands. For the quasi-quadpol configurations, we also computed the total error, which is due to Faraday rotation and the polarimetric interferometric phase difference between the polarization of the $-$ and the $+$ band, $\Delta\phi$. This total error of the corrected phase, ${}_T\delta\phi^c$, was obtained by setting the error in ϕ^+ to ${}_T\delta\phi^+ = {}_F\delta\phi^+ - \Delta\phi$.

IV. RESULTS

A. Co-pol phase errors

The co-pol phase errors induced by Faraday rotation are expected to be small or moderate unless ionospheric Faraday rotation is exceptionally large (Fig. 2a–d). The predicted magnitude of ${}_F\delta\phi$ at HH remains below 3°, or 1 mm, for an increase in Faraday rotation from $\chi_1 = 0°$ to $\chi_2 = 3°$ and 10°. It is only when the second Faraday rotation angle is extremely large, $\chi_2 = 30°$ that $|{}_F\delta\phi|$ in excess of 6° (2 mm) are predicted. It is not only the difference in Faraday rotation that matters. The errors over croplands are appreciable (Fig. 2d) even when the Faraday rotation angles for the two acquisitions are identical but very large, $\chi_1 = \chi_2 = 30°$.

The errors are most pronounced for sparsely vegetated slopes and for agricultural fields. In sparsely vegetated terrain, large phase errors are predominantly associated with polarimetric leakage. The polarimetric leakage error ${}_F\delta\phi^{\mathrm{pol}}$ from a phase-invariant approximation $\mathbf{\Omega}'$ can largely explain the spatial patterns of ${}_F\delta\phi$ in hilly terrain in the San Francisco Bay area (Fig. 3a–b). The dominance of polarimetric leakage also applies to bare surfaces observed at grazing incidence angles. Large negative values ${}_F\delta\phi \sim -45°$, corresponding to deformation errors of 15 mm, prevail for maximum Faraday rotation $\chi_2 = 30°$ (Fig. 3a–b). The large magnitudes are associated with $\arg(\Sigma_{12}) \sim -140°$ and a high polarimetric correlation of ∼0.8. Over agricultural fields during the growing season, the errors vary from field to field in a way that can largely but not entirely be explained by polarimetric leakage (Fig. 4a–b). Phase diversity also contributes to the errors, as the $\mathrm{HH}--\mathrm{VV}$ phase difference exceeds 90° in magnitude in several fields in Fig. 4f). The contribution of phase diversity to the Faraday-induced errors over croplands is evident for $\chi_1 = \chi_2$ (Fig. 2d).

B. Cross-pol phase errors

Faraday rotation can readily induce substantial cross-pol phase errors. For $\chi_1 = 0°$ and small $\chi_2 = 3°$, the predicted magnitudes are shown in Fig. 5 to reach values up to 6°, or 2 mm. For strong and maximum Faraday rotation in the second acquisition, the deformation errors can exceed 10 mm. Errors of comparable magnitude are also obtained when the Faraday rotation is very large but constant.

Particularly large errors are expected in moderate to high-relief terrain. For the sparsely vegetated rolling terrain in in Fig. 3, the error is closely associated with topography and can largely be explained by polarimetric leakage predicted using a phase-invariant $\mathbf{\Omega}'$. The error sign changes with the direction of the azimuth slopes, as predicted by (13) for polarimetric leakage errors.

Even in flat terrain such as that in Fig. 4, polarimetric leakage and phase diversity can induce substantial ${}_F\delta\phi_{\mathrm{HV}}$. Despite the low relief, the ρ_{13} polarimetric coherence in Fig. 4e indicates prominent deviations from reflection symmetry across $\mathcal{P}_V$ in croplands [23], which enable substantial errors according to (11).

C. Simulated temporal evolution of Faraday-induced errors

The Faraday rotation angle χ derived from the IGS TEC product and the simulated errors exhibit complex temporal patterns around the 2002 solar maximum. Figure 6 shows the simulated errors for the two locations annotated in Fig. 3e. Both are sparsely vegetated and on slopes: at HH, the slope faces away from the instrument, while at HV it is mainly in the azimuth direction. As the errors are large for these two locations, the simulations constitute a pessimistic scenario for rolling, sparsely vegetated terrain in California.

The magnitude of the simulated errors is not negligible compared to the desired millimetric geodetic accuracy on semi- to multi-annual time scales. The maximum magnitude differs substantially between the co-pol (HH) and cross-pol (HV) observations. The semi-annual and multi-annual co-pol phase errors are $\sim 5°$, corresponding to 2 mm. The cross-pol errors are 5 times as large.

The temporal patterns differ between the two polarizations. This can be explained by the contrasting dependence of the Faraday-induced errors on χ. At HH, the second-order impact (Tab. I) of χ i) emphasizes the peak TEC ($\chi = 16°$) in 2002 and ii) dampens the annual variations at low TEC after 2004.

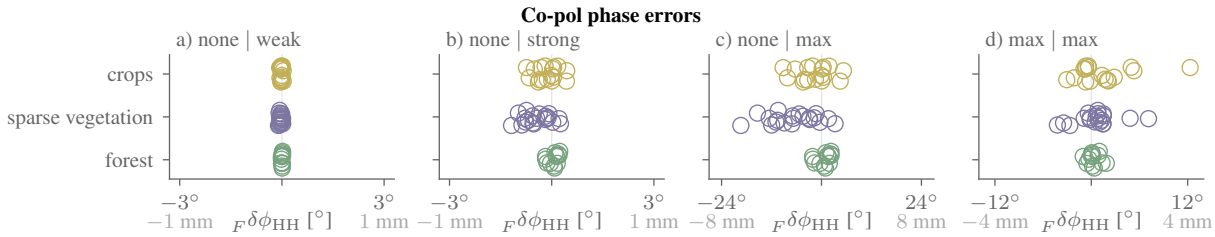

Fig. 2. Faraday-induced phase errors at HH across multiple regions of interest for four different Faraday rotation combinations $\chi_1 \mid \chi_2$ (none, weak, strong, and max are 0°, 3°, 10°, and 30°, respectively). The corresponding deformation error is shown in gray.

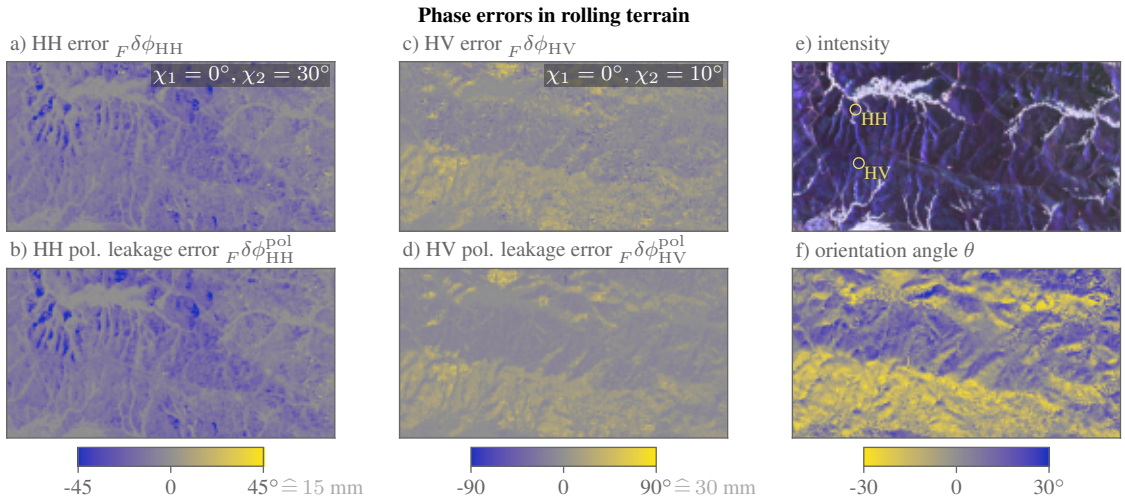

Fig. 3. Faraday-induced phase errors in rolling, predominantly sparsely vegetated terrain near Vallejo, California. The look direction is from the left. a) Error in HH for maximum Faraday rotation $\chi_2 = 30°$; b) HH error predicted by polarimetric leakage using a phase-invariant approximation; c–d) same as a–b) but in HV for strong Faraday rotation $\chi_2 = 10°$; e) Pauli RGB composite showing sparsely vegetated hillslopes and ridges in dark, blueish tones and densely vegetated valleys in white, while the yellow circles indicate the locations shown in Fig. 6; f) polarimetric orientation angle θ.

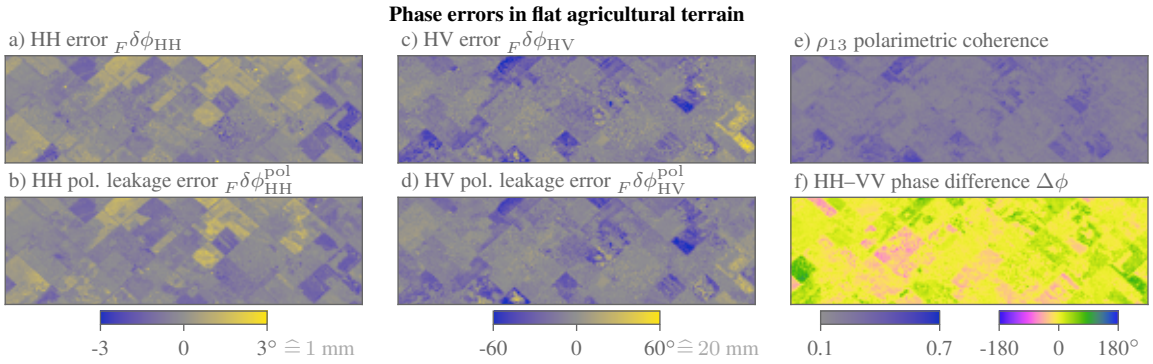

Fig. 4. Faraday-induced phase errors in a flat agricultural landscape near Carman, Winnipeg. The look direction is from below. a, c) Error in HH and HV respectively for strong Faraday rotation $\chi_2 = 10°$ while $\chi_1 = 0°$; b, d) polarimetric leakage errors predicted from a phase-invariant approximation; e) elevated ρ_{13} [-] for certain fields despite the low relief; f) HH–VV interferometric phase difference can be substantial for rapidly changing crops.

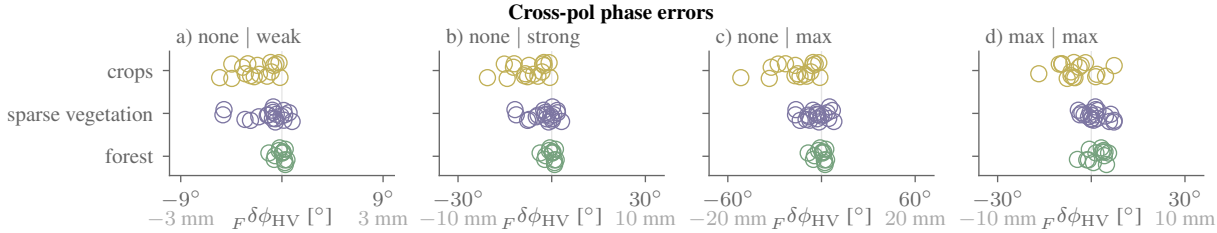

Fig. 5. Faraday-induced phase errors at HV across multiple regions of interest for the same four different Faraday rotation combinations $\chi_1 \mid \chi_2$ as in Fig. 2

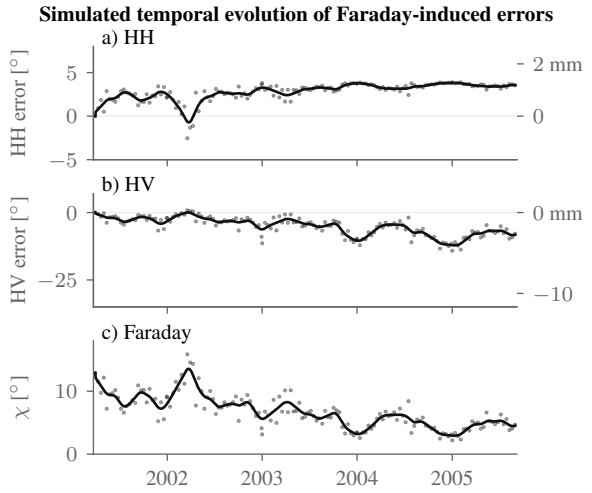

Fig. 6. Simulated Faraday-induced phase errors in California around the 2002 solar maximum for the two locations shown in Fig. 3e. The errors are exclusively due to polarimetric leakage because of the phase-invariant $\mathbf{\Omega}$. a) Simulated HH phase ${}_F\delta\phi^{\mathrm{pol}}_{\mathrm{HH}}$ (left) and displacement error (right); b) same for HV; c) Faraday angle χ estimated from the IGS ionospheric TEC product. The markers show the respective values at an interval of 11 days; the line is a smoothed monthly estimate.

Intuitively, the second-order scaling in Eq. 10 is equivalent to the product of the mean χ and their difference $\Delta\chi$. For a large initial $\chi_1 = 13°$, the second-order error thus i) emphasizes $\Delta\chi$ when both χ are large, and ii) dampens the influence of $\Delta\chi$ when the mean is small. Conversely, the leading first-order term at HV is i) less sensitive to the initial increase in χ from 2001 to 2002, but it ii) amplifies the large difference to the TEC minima after 2004, aided by deviations from purely first-order scaling. To summarize, the Faraday-induced errors can exhibit complex patterns across time scales.

D. Split-spectrum errors

The errors in the ionospherically corrected phase associated with uncompensated Faraday rotation are generally of comparable magnitude to those in the uncorrected phase when the same polarization is used for the upper and lower band (Fig. 7).

For the co-pol channel HH, the error in the corrected phase, ${}_F\delta\phi^c$, is on the order of 2° for strong Faraday rotation ($\chi_1 = 0°$ and $\chi_2 = 10°$). It is thus substantially smaller than the inherent ionospheric phase ambiguity of $\Gamma = 20°$. For maximum Faraday rotation $\chi_2 = 30°$, the errors can exceed those of the uncorrected phase, reaching values of up to 60°, or 20 mm.

For the cross-pol channel HV, the predicted error ${}_F\delta\phi^c$ can exceed 10° for certain croplands at $\chi_2 = 10°$. For maximum $\chi_2 = 30°$, the areas studied are subject to a compensation effect in that the ${}_F\delta\phi_c$ decrease in magnitude (and sometimes change sign) for increasing χ_2.

The quasi-quadpol split-spectrum ionospheric correction is severely compromised (Fig. 8). For the co-pol HH–VV band combination, the total errors ${}_T\delta\phi^c$ commonly exceed 12 cm in Fig. 8a. The errors due to Faraday rotation alone are an order of magnitude smaller (panel b). The large total errors are induced by HH–VV phase differences $\gtrapprox 20°$, which get amplified in the split spectrum correction. For the cross-pol HV–VH combination, the situation is different because the phase differences ϕ_{HV} and ϕ_{VH} are identical for reciprocal targets without Faraday rotation. The errors, which are exclusively due to Faraday rotation, nevertheless commonly exceed 360°, or 12 cm, in Fig. 8c–d.

V. Discussion

A. Magnitude and nature of Faraday-induced phase errors

In the co-polar channels, Faraday-induced interferometric phase errors are often, but not always, small. For both the observed phase (Fig. 2a–b, Fig. 6) and the split-spectrum ionospherically corrected phase (Fig. 7a), they are predicted to generally remain $\lessapprox 5°$, or 2 mm at L-band over a solar cycle. However, our analyses reveal two factors that can conceivable induce larger errors. First, barely vegetated slopes facing away from the radar and other locations whose polarimetric scattering characteristics (large imaginary part of the Pauli 12 component; 10) promote elevated Faraday-induced phase errors due to polarimetric leakage. Second, exceptionally large TEC values, which may occur during strong solar maxima. The associated Faraday rotation angles of up to 30° (Fig. 2c–d) induce substantial errors of ∼5 mm.

For the cross-pol channel, Faraday-induced interferometric phase errors are a major concern (Fig. 5). The magnitude of the ${}_F\delta\phi$ errors can exceed 30°, or 10 mm, even for Faraday rotation that is not exceptionally strong. Sparsely vegetated high-relief terrain is prone to large errors, as the errors contain a topographic signature induced by polarimetric leakage (Fig. 3).

B. Relevance for measuring deformation

The Faraday-induced phase errors in the co-pol channels compel attention in geodetic analyses of deformation, chiefly for three reasons.

First, their magnitudes of ∼2 mm on semi- to multi-annual time scales (co-pol; Fig. 6b) are comparable to the accuracy requirements for the NISAR mission, which are 2 mm/year for secular deformation rates [9]. On shorter time scales, the errors may reach ∼1 cm for very large peak TEC and χ during a solar maximum (Fig. 2d, 3a).

Second, the temporal patterns, with pronounced variability on subseasonal and (semi)-annual time scales as well as persistent longer-term trends (Fig. 6), mimic those of deformation processes such as landslides or aseismic creep. They can thus systematically distort geophysical model inversions and interpretations.

Third, these systematic errors exhibit complex spatial patterns. Their strong association with relief and landcover mimics that of deformation processes such as solifluction. In contrast to other atmospheric errors, the ${}_F\delta\phi$ errors can exhibit sharp boundaries (Fig. 3–4) because the ionospheric patterns are modulated by surface characteristics. Simple spatial high-pass filtering or corrections with sparse GNSS stations cannot mitigate the errors.

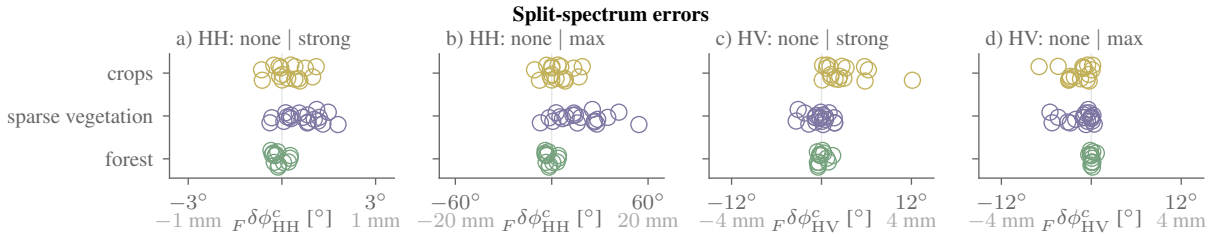

Fig. 7. Faraday-induced errors in the split-spectrum ionospherically corrected phase at a–b) HH and c–d) HV across multiple regions of interest. The Faraday rotation combinations $\chi_1 \mid \chi_2$ overlap with those in Fig. 2

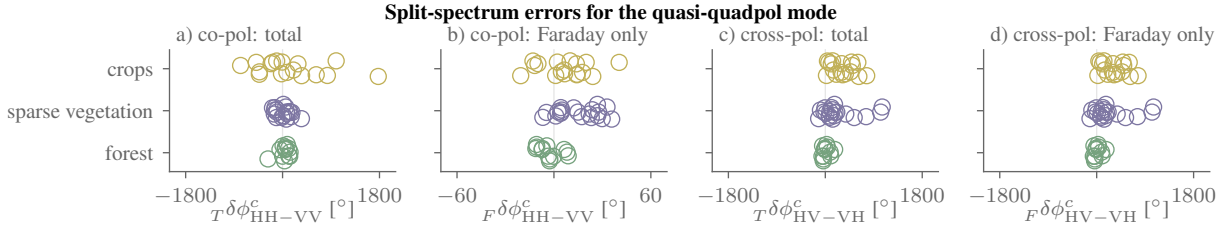

Fig. 8. Faraday-induced errors in the split-spectrum ionospherically corrected phase in the quasi-quadpol mode for $\chi_1 = 0°$ (none) | $\chi_2 = 10°$ (strong). a and c) show the total errors for the HH–VV and the HV–VH band combinations, respectively. b and d) show the error due to Faraday rotation alone for the same combinations. Panels c) and d) are identical because reciprocity was enforced.

In summary, the error magnitudes in the co-pol channels are large enough to warrant consideration, compounded by their pernicious spatiotemporal characteristics.

C. Mitigating Faraday-induced errors in geodetic analyses

It would be desirable to correct the errors, but there is insufficient information to do so rigorously for single-pol and dual-pol data [10], [2]. Even if the Faraday rotation were known accurately, error correction requires estimates of interferometric scattering terms such as Ω_{12} that are unobserved and difficult to predict [15].

A less ambitious goal than error correction is to flag large Faraday-induced errors. Such flagging needs to account for both factors conducive to large errors: elevated TEC and adverse scattering characteristics. Discarding entire scenes with elevated TEC irrespective of the scattering characteristics is akin to throwing out the baby with the bath water. The example of the persistently elevated TEC during the 2002 solar maximum in Figure 6 illustrates that not all compromised scenes can meaningfully be discarded.

Error correction and flagging of single and dual-pol observations is potentially amenable to statistical approaches. The interferometric phase differences between the co-pol and the cross-pol channels are promising predictors. We expect that the predictive skill of statistical correction models will benefit from external ionospheric, land cover, and topographic information (cf. Fig. 3). Another promising avenue is the combination with higher-frequency data such as C-band observations from Sentinel-1.

The best way to avoid Faraday-induced deformation errors is to use quad-pol observations [8]. The error can be removed reliably [2], [19]. Hybrid-pol acquisitions – in which a circularly polarized wave is transmitted – are also robust to Faraday-induced phase errors. This is because Faraday rotation does not add target-dependent phase errors provided one of the circular polarizations is used on receive [10]. In summary, quad-pol and hybrid-pol modes warrant consideration at L-band because they are robust to Faraday-induced deformation errors.

VI. Conclusions

Our theoretical and observational analyses show that phase errors induced by uncompensated Faraday rotation constitute an important and hitherto neglected error in interferometric deformation measurements. Over a solar cycle, the magnitude is generally smaller than 2 mm in the co-pol channels at L-band. However, for surfaces with adverse scattering characteristics, it exceeded 5 mm in the worst-case scenario (intense solar maximum) we simulated. The cross-pol channel is more prone to severe errors, which can exceed several centimeters.

These errors are systematic, as they can add up and persist over time. Their temporal characteristics, such as pronounced seasonal and quasi-decadal variability, are similar to those of common deformation processes. The errors are further strongly associated with the topography and land cover because they result from the modulation of ionospheric delays by surface scattering characteristics. They can largely be attributed to a leakage of polarimetric phases into the interferometric phase. Even when these errors remain subtle ($\sim 6°$ or 2 mm at L band), their systematic nature makes the spurious Faraday-induced patterns prone to being misinterpreted as deformation.

These errors cannot rigorously be corrected for in single- and dual-pol modes because they depend on unobserved quantities. Statistical detection and mitigation approaches thus appear to be a promising avenue for error mitigation. The best and most rigorous way to avoid these errors is to use quad-pol, or hybrid, observations. In absence of quad-pol observations,

the Faraday-induced deformation errors deserve to be included in error budgets and accounted for in quantitative analyses.

VII. Appendix: Invariance / diversity of the interferometric phase

To describe how the interferometric phase formed from the interferometric $\mathbf{\Omega}$, depends on the polarimetric functional $\mathbf{w}^\dagger$. We speak of invariance of the phase when for any two non-zero polarimetric functionals $\mathbf{w}_A^\dagger$ and $\mathbf{w}_B^\dagger$

$$\arg\left(\mathbf{w}_A^\dagger \mathbf{\Omega} \mathbf{w}_A\right) = \arg\left(\mathbf{w}_B^\dagger \mathbf{\Omega} \mathbf{w}_B\right) . \tag{16}$$

We refer to such an $\mathbf{\Omega}$ as phase invariant. If the condition is not fulfilled, we say $\mathbf{\Omega}$ exhibits phase diversity. The condition in (16) requires that $\mathbf{w}^\dagger \mathbf{\Omega} \mathbf{w} \neq 0$ for $\mathbf{w}_A^\dagger$ and $\mathbf{w}_B^\dagger$. We treat functionals for which $\mathbf{w}^\dagger \mathbf{\Omega} \mathbf{w} = 0$ as separate cases, i.e. they are assumed not to break invariance in and of themselves.

Invariance of the phase

$\mathbf{\Omega}$ is phase invariant if and only if $\mathbf{\Omega}$ can be written as $\mathrm{e}^{\mathrm{i}\tilde{\phi}}\tilde{\mathbf{\Omega}}$ where $\tilde{\mathbf{\Omega}} = \tilde{\mathbf{\Omega}}^\dagger$ is positive semi-definite.

Proof

If: Provided $\mathbf{w}^\dagger \mathbf{\Omega} \mathbf{w} \neq 0$

$$\phi_{\mathbf{w}^\dagger} = \arg\left(\mathrm{e}^{\mathrm{i}\tilde{\phi}} \underbrace{\mathbf{w}^\dagger \tilde{\mathbf{\Omega}} \mathbf{w}}_{>0}\right) = \tilde{\phi} ,$$

which is independent of $\mathbf{w}^\dagger$.

Only if: Pick a $\mathbf{w}_\heartsuit^\dagger$ such that the magnitude of $\mathbf{w}_\heartsuit^\dagger \mathbf{\Omega} \mathbf{w}_\heartsuit \equiv a_\heartsuit \mathrm{e}^{\mathrm{i}\phi_\heartsuit}$ is strictly greater than zero, i.e. $a_\heartsuit > 0$. If one cannot pick such a $\mathbf{w}_\heartsuit^\dagger$, this can be shown to imply that $\mathbf{\Omega}$ is the zero matrix, in which case interferometric phases are not defined. Having found $\mathbf{w}_\heartsuit^\dagger$, we can write for general $\mathbf{w}^\dagger$

$$\phi_{\mathbf{w}^\dagger} = \arg\left(\mathrm{e}^{\mathrm{i}\phi_\heartsuit} \underbrace{\mathbf{w}^\dagger \mathrm{e}^{-\mathrm{i}\phi_\heartsuit} \mathbf{\Omega} \mathbf{w}}_{m(\mathbf{w}^\dagger)}\right) . \tag{17}$$

Invariance of the phase implies that $m(\mathbf{w}^\dagger)$ must be real and ≥ 0. This in turn implies that $\mathrm{e}^{-\mathrm{i}\phi_\heartsuit}\mathbf{\Omega}$ is Hermitian (real) positive semidefinite (≥ 0). For any phase-invariant $\mathbf{\Omega}$, it thus follows that $\phi_\heartsuit = \tilde{\phi}$ and unique (modulo 2π). Furthermore, $\tilde{\mathbf{\Omega}} = \mathrm{e}^{-\mathrm{i}\tilde{\phi}}\mathbf{\Omega}$.

A complementary way of interpreting invariance is by relation to the coherence region and the numerical range [24], [25] of $\mathbf{\Omega}$, $W(\mathbf{\Omega})$. The set of all valid $\phi_{\mathbf{w}^\dagger}$ is the image of $W(\mathbf{\Omega})$ under the argument function. If it is to collapse to a single value (invariance), $W(\mathbf{\Omega})$ must be contained in a ray. This in turn is equivalent to $\mathbf{\Omega}$ being a normal matrix whose eigenvalues all have the same argument [26], viz. $\mathbf{\Omega} = \mathrm{e}^{\mathrm{i}\tilde{\phi}}\tilde{\mathbf{\Omega}}$ if we allow for zero eigenvalues.

VIII. Appendix II: Accumulation of polarimetric leakage errors

We show that the polarimetric leakage errors are temporally persistent across chains of interferograms. Even if the Faraday rotation change and hence the error is small for short temporal baselines, long-term changes in Faraday rotation will induce systematic long-term errors.

We assume the phase-invariant $\mathbf{\Omega} = \tilde{\mathbf{\Omega}}$ is time invariant for nearest-neighbour interferograms. The proportionality constant of the leading-order error from (10) and (13) is constant. Referreng to it by β, the total error when adding up nearest-neighbour interferograms

$$\begin{aligned} {}_F\delta\phi^{1\,2} + \cdots + {}_F\delta\phi^{(K-1)\,K} &= \sum_{k=1}^{K-1} \beta(\chi_k^n - \chi_{k+1}^n) + o(\chi^n) \\ &= \beta(\chi_1^n - \chi_K^n) + o(\chi^n) , \end{aligned} \tag{18}$$

so that up to the leading order n (1 for cross-pol, 2 for co-pol), this would be equal to $\phi^{1\,K}$ if the latter had the same $\tilde{\Omega}$. To arbitrary order of accuracy, it is the single-interferogram error for an effective phase-diverse $\mathbf{\Omega}^e$

$$\mathbf{\Omega}^e = \tilde{\mathbf{\Omega}}^{\frac{1}{2}} \mathbf{l}_2 \mathbf{l}_2^\dagger \cdots \mathbf{l}_{K-1} \mathbf{l}_{K-1}^\dagger \tilde{\mathbf{\Omega}}^{\frac{1}{2}} , \tag{19}$$

where $\mathbf{l}_k \equiv \tilde{\mathbf{\Omega}}^{\frac{1}{2}} \mathbf{R}_F^T(\chi_k)\mathbf{w}$, and where $\tilde{\mathbf{\Omega}}^{\frac{1}{2}}$ is the Hermitian square root. Because variable χ_k maps variable polarimetric components in $\tilde{\mathbf{\Omega}}^{\frac{1}{2}}$ to $\mathbf{l}_k$, the polarimetric leakage errors do not add up perfectly in general. The non-additive nature can be interpreted as a breaking of phase closure [27] due to polarimetric leakage. Conversely, for rank-one interferometric scatterers $\tilde{\mathbf{\Omega}} = \mathbf{a}\mathbf{a}^\dagger$, the errors add up.

IX. Acknowledgements

UAVSAR data courtesy NASA/JPL-Caltech.

References

[1] P. A. Wright, S. Quegan, N. S. Wheadon, and C. D. Hall, "Faraday rotation effects on L-band spaceborne SAR data," *IEEE Transactions on Geoscience and Remote Sensing*, vol. 41, pp. 2735–2744, Dec 2003.

[2] F. J. Meyer and J. B. Nicoll, "Prediction, detection, and correction of Faraday rotation in full-polarimetric L-band SAR data," *IEEE Transactions on Geoscience and Remote Sensing*, vol. 46, pp. 3076–3086, Oct 2008.

[3] E. V. Appleton and G. Builder, "The ionosphere as a doubly-refracting medium," *Proceedings of the Physical Society*, vol. 45, pp. 208–220, mar 1933.

[4] G. Hartmann and R. Leitinger, "Range errors due to ionospheric and tropospheric effects for signal frequencies above 100 MHz," *Bulletin géodésique*, vol. 58, pp. 109–136, 1984.

[5] J. R. Jokipii and I. Lerche, "Faraday rotation, dispersion in pulsar signals, and the turbulent structure of the galaxy," *Astrophysical Journal*, vol. 157, no. 3, pp. 1137–1145, 1969.

[6] A. Freeman and S. S. Saatchi, "On the detection of Faraday rotation in linearly polarized L-band SAR backscatter signatures," *IEEE Transactions on Geoscience and Remote Sensing*, vol. 42, pp. 1607–1616, Aug 2004.

[7] R. Z. Schneider and K. Papathanassiou, "Pol-dinSAR: polarimetric SAR differential interferometry using coherent scatterers," in *2007 IEEE International Geoscience and Remote Sensing Symposium*, pp. 196–199, July 2007.

[8] E. J. M. Rignot, "Effect of faraday rotation on L-band interferometric and polarimetric synthetic-aperture radar data," *IEEE Transactions on Geoscience and Remote Sensing*, vol. 38, no. 1, pp. 383–390, 2000.

[9] K. Kellogg, P. Hoffman, S. Standley, S. Shaffer, P. Rosen, W. Edelstein, C. Dunn, C. Baker, P. Barela, Y. Shen, A. M. Guerrero, P. Xaypraseuth, V. R. Sagi, C. V. Sreekantha, N. Harinath, R. Kumar, R. Bhan, and C. V. H. S. Sarma, "NASA-ISRO synthetic aperture radar (NISAR) mission," in *2020 IEEE Aerospace Conference*, pp. 1–21, 2020.

[10] S. H. Bickel and R. H. T. Bates, "Effects of magneto-ionic propagation on the polarization scattering matrix," *Proceedings of the IEEE*, vol. 53, no. 8, pp. 1089–1091, 1965.

[11] G. Gomba, A. Parizzi, F. De Zan, M. Eineder, and R. Bamler, "Toward operational compensation of ionospheric effects in SAR interferograms: The split-spectrum method," *IEEE Transactions on Geoscience and Remote Sensing*, vol. 54, pp. 1446–1461, March 2016.

[12] S. Zwieback and I. Hajnsek, "Influence of vegetation growth on the polarimetric DInSAR phase diversity – implications for deformation studies," *IEEE Trans. Geosc. Remote Sens.*, vol. 54, no. 5, pp. 3070–3082, 2016.
[13] S. R. Cloude and E. Pottier, "A review of target decomposition theorems in radar polarimetry," *IEEE Transactions on Geoscience and Remote Sensing*, vol. 34, pp. 498–518, March 1996.
[14] S. R. Cloude and K. P. Papathanassiou, "Polarimetric SAR interferometry," *IEEE Transactions on Geoscience and Remote Sensing*, vol. 36, pp. 1551–1565, Sep. 1998.
[15] S. R. Cloude, D. G. Goodenough, H. Chen, Y. S. Rao, and W. Hong, "Pauli phase calibration in compact polarimetry," *IEEE Journal of Selected Topics in Applied Earth Observations and Remote Sensing*, vol. 11, no. 12, pp. 4906–4917, 2018.
[16] J. Lee and T. L. Ainsworth, "The effect of orientation angle compensation on coherency matrix and polarimetric target decompositions," *IEEE Transactions on Geoscience and Remote Sensing*, vol. 49, pp. 53–64, Jan 2011.
[17] R. Brcic, A. Parizzi, M. Eineder, R. Bamler, and F. Meyer, "Estimation and compensation of ionospheric delay for SAR interferometry," in *2010 IEEE International Geoscience and Remote Sensing Symposium*, pp. 2908–2911, July 2010.
[18] V. Brancato, F. Liebisch, and I. Hajnsek, "Impact of plant surface moisture on differential interferometric observables: A controlled electromagnetic experiment," *IEEE Transactions on Geoscience and Remote Sensing*, vol. 55, no. 7, pp. 3949–3964, 2017.
[19] J. S. Kim, K. P. Papathanassiou, R. Scheiber, and S. Quegan, "Correcting distortion of polarimetric SAR data induced by ionospheric scintillation," *IEEE Transactions on Geoscience and Remote Sensing*, vol. 53, pp. 6319–6335, Dec 2015.
[20] A. G. Fore, B. D. Chapman, B. P. Hawkins, S. Hensley, C. E. Jones, T. R. Michel, and R. J. Muellerschoen, "UAVSAR polarimetric calibration," *IEEE Transactions on Geoscience and Remote Sensing*, vol. 53, pp. 3481–3491, June 2015.
[21] M. Hernández-Pajares, J. M. Juan, J. Sanz, R. Orus, A. Garcia-Rigo, J. Feltens, A. Komjathy, S. C. Schaer, and A. Krankowski, "The IGS VTEC maps: a reliable source of ionospheric information since 1998," *Journal of Geodesy*, vol. 83, pp. 263–275, 2009.
[22] S. Zwieback, X. Liu, S. Antonova, B. Heim, A. Bartsch, J. Boike, and I. Hajnsek, "A statistical test of phase closure to detect influences on DInSAR deformation estimates besides displacements and decorrelation noise: Two case studies in high-latitude regions," *IEEE Transactions on Geoscience and Remote Sensing*, vol. 54, pp. 5588–5601, Sept 2016.
[23] S. Zwieback and I. Hajnsek, "Statistical tests for symmetries in polarimetric scattering coherency matrices," *IEEE Geoscience and Remote Sensing Letters*, vol. 11, pp. 308–312, Jan 2014.
[24] M. Neumann, L. Ferro-Famil, and A. Reigber, "Pol-InSAR coherence set theory and application," in *6th European Conference on Synthetic Aperture Radar*, 2006.
[25] Y. Cui, Y. Yamaguchi, H. Yamada, and S. Park, "PolInSAR coherence region modeling and inversion: The best normal matrix approximation solution," *IEEE Transactions on Geoscience and Remote Sensing*, vol. 53, pp. 1048–1060, Feb 2015.
[26] F. D. Murnaghan, "On the field of values of a square matrix," *Proceedings of the National Academy of Sciences*, vol. 18, pp. 246–248, 1932.
[27] F. De Zan, M. Zonno, and P. Lopez-Dekker, "Phase inconsistencies and multiple scattering in SAR interferometry," *IEEE Transactions on Geoscience and Remote Sensing*, vol. 53, pp. 6608 – 6616, December 2015.